Taylor & Francis
Taylor & Francis Group

REPORT

🔓 OPEN ACCESS | Check for updates

Structural and biochemical differences between non-catalytic and catalytic antibodies

Taizo Uda [a,b], Ryuichi Kato[c], Yasuteru Shigeta[d], Shun Hirota[e], Jun Kobayashi[c], Hisashi Yoshida[c], Masato Tsuyuguchi[c], Kowit Hengphasatporn[d], Moe Tsujita[f,g], Hiroaki Taguchi [b], and Emi Hifumi [a,g]

aResearch Center for GLOBAL/LOCAL Infectious Diseases, Oita University, Oita-shi, Oita, Japan; bFaculty of Pharmaceutical Sciences, Suzuka University of Medical Science, Suzuka, Japan; cStructural Biology Research Center, Photon Factory, Institute of Materials Structure Science, High Energy Accelerator Research Organization (KEK), Tsukuba, Ibaraki, Japan; dCenter for Computational Sciences, University of Tsukuba, Tsukuba, Ibaraki, Japan; eDivision of Materials Science, Graduate School of Science and Technology, Nara Institute of Science and Technology, Takayama, Ikoma, Nara, Japan; fGraduate School of Engineering, Oita University, Oita-shi, Oita, Japan; gInstitute for Research Management, Oita University, Oita-shi, Oita, Japan

ABSTRACT

A conventional antibody can be converted into its catalytic counterparts by deleting Pro95 in the CDR-3 of human and mice antibody light chains, as previously reported. T99wt is a naturally occurring human antibody light chain that we transformed into its catalytic antibody using Pro95 deletion. In peptidase activity tests, T99wt exhibited a low catalytic activity against a synthetic peptide Arg-pNA and hardly cleaved amyloid-β peptide. In contrast, the engineered variant (T99-Pro95(-)) demonstrated significant catalytic activity, effectively cleaving both Arg-pNA substrate and amyloid-β peptides. In this study, the structural basis for the acquisition of enzymatic function through Pro95 deletion in the CDR-3 region of the light chain was elucidated using X-ray crystallography and molecular dynamics (MD) simulations. X-ray crystallography revealed that Pro95 deletion substantially reduces the distance between Asp1 and His93—key residues for catalytic activity – from 9.56 Å in T99wt to 3.84 Å in T99-Pro95(-). The observed decrease in distance indicates a strong interaction between Asp1(Oδ1) and His93(Nε2), contributing to the formation of an active site in T99-Pro95(−). MD simulations revealed that the entire structure exhibits slight fluctuations and adopts various configurations upon the removal of Pro95. In particular, when His residues in the catalytic region are fully deprotonated, Asp1, His93, and Ser27a transiently come into close proximity, enabling the formation of a functional catalytic triad. Catalytic antibodies can be made starting from just the amino acid sequence of a desired mAb, which may be available in databases such as OAS or IMGT. Therefore, our finding represents a significant technological advancement.

Introduction

Naturally occurring catalytic antibodies that hydrolyze targeted peptides,[1,2] nucleotides,[3–5] physiologically active molecules,[6–10] and viral and bacterial antigenic proteins,[11–22] have been reported. In addition, interesting applications based on catalytic antibodies have been reported. The catalytic antibody UA-15 L degrading *Helicobacter pylori* urease possesses the ability not only to eliminate the enzymatic activity of urease, but to also reduce the predominance of *H. pylori* in the mouse stomach by oral administration.[23] Paul *et al.* succeeded in clearing amyloid-beta (Aβ) aggregates deposited in the brains of mice using an anti-Aβ catalytic antibody.[14] Such features can be substantially more useful than those of non-catalytic antibodies. However, considerable time and effort are required to produce catalytic antibodies, making their application in various fields challenging. To address this limitation, we developed an evolutionary method for preparing catalytic antibodies, in which a conventional antibody can be converted into its catalytic counterpart by genetically deleting Pro95 in the CDR-3 region of the light chain. Using this approach, we successfully conferred or enhanced catalytic activity

in conventional antibody light chains.[24] This finding is particularly significant, as it enables the generation of catalytic antibodies from existing monoclonal antibodies, of which many thousands have been developed since the hybridoma production method was reported by Köhler and Milstein.[25]

Nonetheless, a crucial question remains: how does the converted catalytic antibody acquire its catalytic function? Specifically, how is the catalytic site formed and completed?

Many studies on the catalytic sites have reported to date. A catalytic triad composed of Asp-Ser-His[2,8,16,26] or a dyad[27] of His-Ser has been proposed as potential catalytic sites, whereas an alternative triad composed of Arg-Thr-Gln, which cleaves the PD-1 molecule, was recently discovered.[28] In this study, we investigated the properties of naturally occurring T99wt, which is a human antibody light chain, and its genetically deleted Pro95 variant ((T99-Pro95(-)). Interestingly, the typical amino acids (Asp1-Ser27a-His93) are present in both sequences. However, the wild-type (T99wt) did not show a catalytic function, whereas the Pro95-deleted variant (T99-Pro95(-)) exhibited catalytic function.

Catalytic antibodies have been more frequently identified in antibody light chains than in intact full-length antibodies. This research trend is based on several key findings: (1) the active site responsible for vasoactive intestinal peptide degradation was first found in the light chain[2]; (2) certain Bence Jones proteins (free human antibody light chains) were discovered to possess peptidase activity[29,30]; and (3) catalytic activity is often observed in dissociated light chains but not in the intact antibody. Furthermore, a study by Okochi et al. demonstrated that catalytic activity present in the light chain can be lost upon association with the heavy chain.[31] For these reasons, we have chosen to focus exclusively on the light chain in our study of catalytic antibodies.

To address the question of how the catalytic site is formed, we investigated the structures of both clones (T99wt and T99-Pro95(-)) using X-ray crystallography and molecular dynamics (MD) simulations, as well as their biochemical features. The distance between Asp1 and His93, which is related to the structure of the catalytic active site, was found to be 9.56 Å when catalytic activity was absent. However, when catalytic activity was present, the distance reduced to 3.84 Å, indicating a strong interaction between Asp1(Oδ1) and His93(Nε2). These results led to two important conclusions: (1) deletion of Pro95 from an antibody light chain generates a favorable catalytic site capable of cleaving the antigen; and (2) since residues such as Asp1, Ser27a, and His93 play critical roles in catalytic function, antibodies possessing these residues have the potential to be converted into catalytic antibodies through the Pro95-deletion strategy.

Results

Amino acid sequences and biochemical features of T99wt and T99-Pro95(-)

T99wt, a human antibody light chain derived from human lymphocytes,[17] belongs to the germline gene Vκ2–29 × 02 in subgroup II. The Pro95 residue was deleted from the CDR-3 region of T99wt to create T99-Pro95(-).[24] The amino acid sequences are shown in Figure 1. The only difference between these two antibody light chains is the presence or absence of the Pro95 residue. However, the two light chains possess substantially different biochemical features.

Peptidase activity

For a synthetic substrate arg-pNA

To evaluate catalytic activity of an antibody or the subunit, Matsuura et al.[29] Durova et al.[32] and Paul et al.[33] used synthetic substrates such as peptide (or amino acid) conjugated with *p*-nitroanilide (pNA) and (7-methoxycoumarin-4-yl)acetyl (MCA). In this study, we used synthetic peptides, such as Arg-pNA (R-pNA), Glu-pNA, Ala-pNA, Phe-Leu-pNA and Gly-Pro-pNA, to estimate the catalytic activity of T99wt and T99-Pro95 (-). Of these, only Arg-pNA (R-pNA), a trypsin-like substrate, was cleaved by the antibody light chain as described below. The chemical structure of R-pNA is displayed in the inset of Figure 2a, with the red arrow indicating the cleavable peptide bond. The time courses of the degradation reaction for R-pNA by T99-Pro95 (-) and T99wt are shown in Figure 2a. The cleavage reaction by T99-Pro95(-) progressed in a time-dependent manner, releasing 2.08 μM of R-pNA at 72 hr. In contrast, T99wt hardly exhibited the cleavage activity, which was comparable with the control (phosphate-buffered saline (PBS)). Notably, the deletion of Pro95 enhanced the catalytic activity by a factor of three.

A kinetic study was performed by varying the R-pNA substrate concentration (50 ~ 400 μM), while keeping the concentration of T99-Pro95(-) constant at 5 μM. The result is presented in Figure 2b, where a Lineweaver – Burk plot is presented. A linear relationship between 1/v and 1/S is observed, suggesting that the degradation by T99-Pro95(-) obeys the Michaelis-Menten equation and the reaction should be enzymatic. The catalytic reaction constant (kcat) and the Michaelis-Menten constant (Km) were 8×10^{-3} min^{-1} and 3.4×10^{-3} M, respectively. These values are comparable with those of catalytic antibody light chain. Matsuura et al. reported that a Bence Jones protein comprising immunoglobulin light chains produced by plasma cells derived from a patient with multiple myeloma exhibited a catalytic efficiency with a kcat of 7×10^{-2} min^{-1} and a Km of 0.21×10^{-4} M for the R-pNA substrate.[29] Hifumi et al. demonstrated that the S38 catalytic antibody light chain degraded R-pNA with a kcat of 4×10^{-3} min^{-1} and a Km of 3.6×10^{-4} M[24]. Durova et al. reported that the L12 light chain cleaved PFR-MCA with a kcat of 2×10^{-3} min^{-1} and a Km of 5.3×10^{-5} M[32].

T99wt:
DIVMTQTPVSLAVTPGQSASISCRSSQSLLHGDGRSYLYWYVQRPGQSPQLLMYEASTRVS
GVPDRFTGSGSGTDFTLKISRVEAEDVGVYYCMQGTHWPGTFGPGTKVDIKRTVAAPSVFI
FPPSDEQLKSGTASVVCLLNNFYPREAKVQWKVDNALQSGNSQESVTEQDSKDSTYSLSST
LTLSKADYEKHKVYACEVTHQGLSSPVTKSFNRGEC

T99-Pro95(-):
DIVMTQTPVSLAVTPGQSASISCRSSQSLLHGDGRSYLYWYVQRPGQSPQLLMYEASTRVS
GVPDRFTGSGSGTDFTLKISRVEAEDVGVYYCMQGTHW–GTFGPGTKVDIKRTVAAPSVFI
FPPSDEQLKSGTASVVCLLNNFYPREAKVQWKVDNALQSGNSQESVTEQDSKDSTYSLSST
LTLSKADYEKHKVYACEVTHQGLSSPVTKSFNRGEC

- ; deletion

Green; CDR-1, Pink, CDR-2, Blue; CDR-3

Figure 1. Amino acid sequences of T99wt and T99-Pro95(-). Full sequences of human antibody light chain T99wt and T99-Pro95(-). The latter was prepared by deleting the Pro95 residue from T99wt.
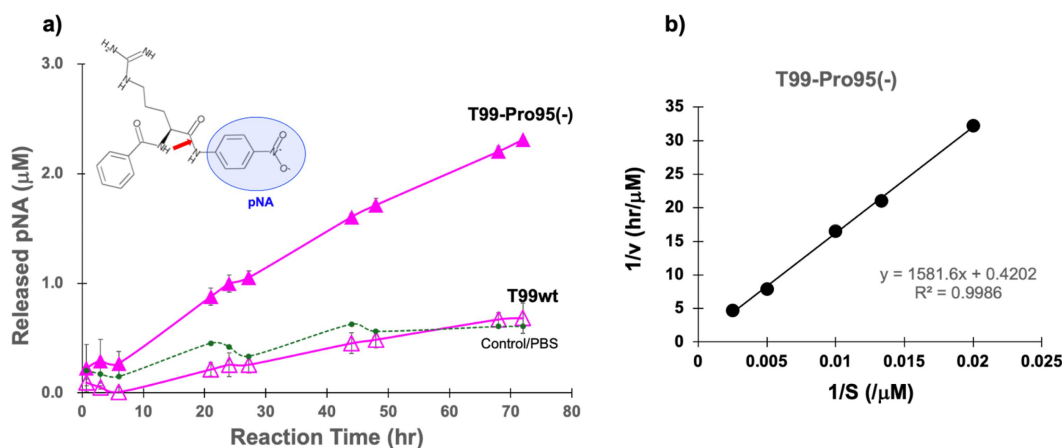
Figure 2. Cleavage assay using a synthetic substrate arg-pNA. (a) Time courses of the cleavage reaction of R-pNA by T99wt and T99-Pro95(-), which were conducted in duplicate. The chemical structure of the substrate Arg-pNA (specifically, Bz-L-Arg-pNA·HCl, abbreviated as R-pNA) is shown in the inset figure, with a red arrow indicating the cleavable peptide bond. T99-Pro95(-) (pink closed triangle) : 5 μM T99wt (pink open triangle): 5 μM R-pNA: 50 μM Control (closed circle with dotted line): PBS without any antibody light chain (*n* = 1) (b) Lineweaver–Burk plot for the cleavage reaction by T99-Pro95(-). [S]: R-pNA, [v]: initial rate, T99-Pro95(-): 5 μM, R-pNA: 50~400 μM A linear relationship between 1/[v] vs. 1/[S] was observed, indicating that degradation of R-pNA obeyed the Michaelis-Menten kinetics, suggesting that the reaction is enzymatic.

For FRET-Aβ and -Tau peptides

Subsequent screening tests of various peptides revealed that T99-Pro95(-) specifically cleaves the Aβ peptide. Accordingly, further investigations were conducted as below.

Alzheimer disease (AD) is the most common form of dementia. The Aβ peptide and Tau protein are known as causative molecules facilitating the development of AD.[34] In this study, the catalytic activity of T99wt and T99-Pro95(-) was analyzed using two chemically synthesized substrates: FRET-Aβ (26–33: MCA-SNKGAIIGK (DNP)rrr-NH2; a region associated with aggregation and oligomer formation) and FRET-Tau peptide (391–408: 7-MCA-EIVYKpSPVVSGDTpSPRHLK (DNP)-NH2;

pS indicates phosphorylated serine; this region is linked to pathogenicity). The chemical structures of FRET-Aβ and FRET-Tau peptides are presented in Figures 3a,c respectively. Details on the synthesis are provided in the Materials and Methods.

Figure 3b presents the time course of the cleavage reaction, demonstrating that the FRET-Aβ peptide was cleaved by T99-Pro95(-) in a time-dependent manner. The peptide bond between Gly and Ala was predominantly hydrolyzed.[24] In contrast, T99wt exhibited minimal cleavage activity toward the FRET-Aβ peptide. The fluorescence intensity (Fu) of T99-Pro95(-) at 72 hours was 12 times higher than that of T99wt.
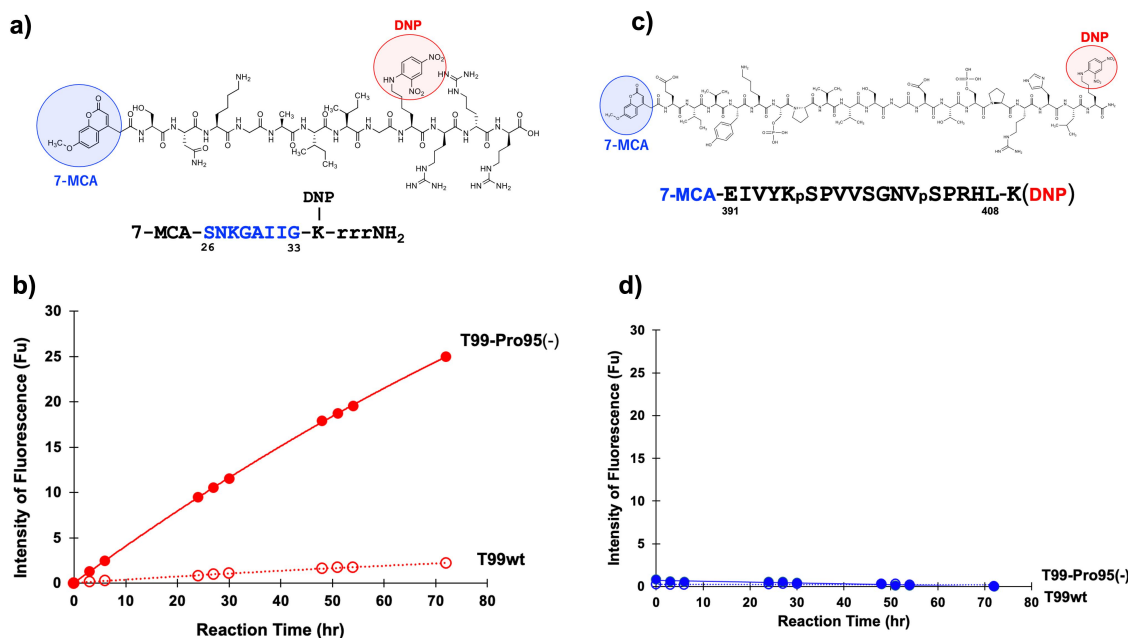

Figure 3. Time course of the cleavage reaction by T99wt and T99-Pro95(-). (a) Chemical structure of FRET-Amyloid-beta (FRET-Aβ) peptide. (b) Time course of degradation of FRET-Aβ by T99-Pro95(-) and T99wt. FRET-Aβ peptide, 25 μM; T99-Pro95(-) (closed circle) and T99wt (open circle), 5 μM; T99-Pro95(-) cleaved FRET-Aβ peptide in a time-dependent manner, while T99wt hardly not. (c) Chemical structure of FRET-Tau (391–408) peptide. (d) Time course of degradation of FRET-Tau by T99-Pro95(-) and T99wt. FRET-Tau peptide, 25 μM; T99-Pro95(-) and T99wt, 5 μM Both T99-Pro95(-) and T99wt light chain did not cleave the FRET-Tau-(391–408) peptide.

In the experiment of FRET-Tau-(391–408) peptide, T99-Pro95 (-), as well as T99wt, did not cleave the peptide (Figure 3d). These results indicate that T99-Pro95(-) possesses the ability to selectively degrade Amyloid-β. The deletion of Pro95 in the light chain confers high catalytic function to the antibody.

Binding affinity to amyloid-beta (Aβ) peptide

The deletion of Pro95 from the light chain could lead to significant structural and biochemical differences. To investigate the immunological characteristics between T99wt and T99-Pro95(-), protein-protein interactions between the antigen and either T99wt or T99-Pro95(-) were analyzed using the Octet N1 system (Sartorius). In the experiment, an Aβ (1–42) peptide with a biotin-tag was used as the antigen to fix on the SA-sensor-chip. Association and dissociation kinetics were determined for each analyte (T99wt or T99-Pro95(-); 0 ~ 1000 nM). The results are presented in Table 1 (sensorgrams are shown in Supporting Information Figure S1a and S1b). Because the binding experiments were completed in two minutes at room temperature, the possibility of degradation of the amyloid-beta (1–42) peptide was considered unlikely. The dissociation constants (K_D) of T99wt and T99-Pro95(-) were 4.43×10^{-8} M and 3.35×10^{-8} M, respectively. The values of ka are 3.73 and 4.03 ($M^{-1}s^{-1}$)(x 10^4) respectively. This difference is less than 10%. The kd values are 1.67 and 1.35 (s^{-1} x 10^{-3}) for each respective clone, representing a difference of approximately 20%. It is assumed that antigen dissociation is more difficult in the Pro-deleted variant, suggesting that the catalytic site may retain the antigen for a longer period compared to the wild type.

The binding affinity of T99-Pro95(-) was similar to that of T99wt.

X-ray crystallography

As described above, catalytic function was observed in T99-Pro95(-) but not in T99wt. To investigate why Pro95 causes this difference, the 3D-structures of both antibody light chains were determined by X-ray crystallography. As the germline gene of T99wt belongs to Vκ2–29 × 02, the Asp1-Ser27a-His93 residues are the most plausible as candidates that generate a catalytic site [326]. Hence, these three residues were the focus of the subsequent structural analysis (data collection and refinement statistics are shown in Supporting Information Table S1).

T99wt

The crystal structure of the T99wt light chain was resolved at a 2.6 Å resolution (PDB code: 8ZNT). Interestingly, eight T99wt molecules were present in the asymmetric unit (ASU) of the T99wt crystal (Figure 4a). The eight molecules can be categorized into two types: bent and straight, as shown in Figure 4b. In spite of the largely different spatial arrangement

of the two structures, the structures of their respective CL and VL domains are nearly identical and overall structures of the CDR regions are also conserved. As previously reported,[24] the assumed catalytic triad consists of Asp1-His93-Ser27a. Hence, the Cα distances among these residues were calculated for the eight molecules to determine any significant differences between those positions. The results are presented in Table 2, where the distances of Cα between Asp1-His93 and Ser27a-His93 are listed. We did not observe any significant differences in the distances between Asp1-His93 in the range of 7.5 to 8.5 Å. Distances between His93-Ser27a were in the range of 9.4 to 10.4 Å. Since the values corresponding to molecule A and G were close to the average of the eight molecules, molecule A was used as the representative structure of T99wt in all subsequent analyses. The crystal structure of molecule A is shown in Figure 4c, where CDR-1 (green), CDR-2 (magenta), and CDR-3 (blue) are shown, along with the three amino acids Asp1, Ser27a, and His93. The distance between Asp1 (Oδ1)-His93 (Nδ1) was 9.56 Å and that between His93 (Nε2) and Ser27a (Oγ) was 6.62 Å.

T99-Pro95(-)

The structure of T99-Pro95 (-) was resolved at a 2.0 Å resolution (PDB code: 8ZNU). In this case, one molecule of T99-Pro95(-) was present in the asymmetric unit of the crystal (Figure 5a). The structure of the variable region of T99-Pro95 (-) is shown in Figure 5b. The distance between Asp1 (Oδ1)-His93 (Nε2) is 3.84 Å and that between His93 (Nε2) and Ser27a (Oγ) is 12.66 Å. The distance between Asp1-His93 of T99-Pro95(-) became shorter by 5.71 Å compared to that of T99wt. In contrast, the distance between His93-Ser27a was prolonged from 6.62 Å (T99wt) to 12.66 Å (T99-Pro95(-). In the case of trypsin (a typical serine protease), the distance between Asp102 (Oδ1)-His57 (Nε2) is 2.67 Å, which is shorter a little than that of T99-Pro95(-) (see supplemental Figure S4).

Comparison of the T99wt and T99-Pro95(-) structures

The structures of the variable region of T99wt and T99-Pro95 (-) were superimposed, as shown in Figure 4c. With regards to the entire structure of both molecules, no significant changes were observed, except for the His93 residue. Based on an enlarged view, the structures of the backbone and CDR-1 for T99wt and T99-Pro95 (-) were highly similar. In contrast, their CDR-3 structures (T99wt: blue; T99-Pro95(-): light blue) were significantly different owing to the lack of a Pro95 residue. Among the Asp1, Ser27a, and His93 (with Ser26 included in the figure as a reference) residues, only His93 exhibited distinct conformational changes, whereas the positions of Asp1, Ser27a, and Ser26 remained almost unchanged. In the T99wt structure, the His93 side chain shifted approximately 3.17 Å (Cα-Cα) and 6.74 Å (Nε2-Nε2) toward Pro95 (to the left in Figure 5c), bringing His93 closer to Asp1. The positions of Ser26 and Ser27a remained consistent, regardless of the

Table 1. Binding kinetics for Amyloid-beta (1–42).

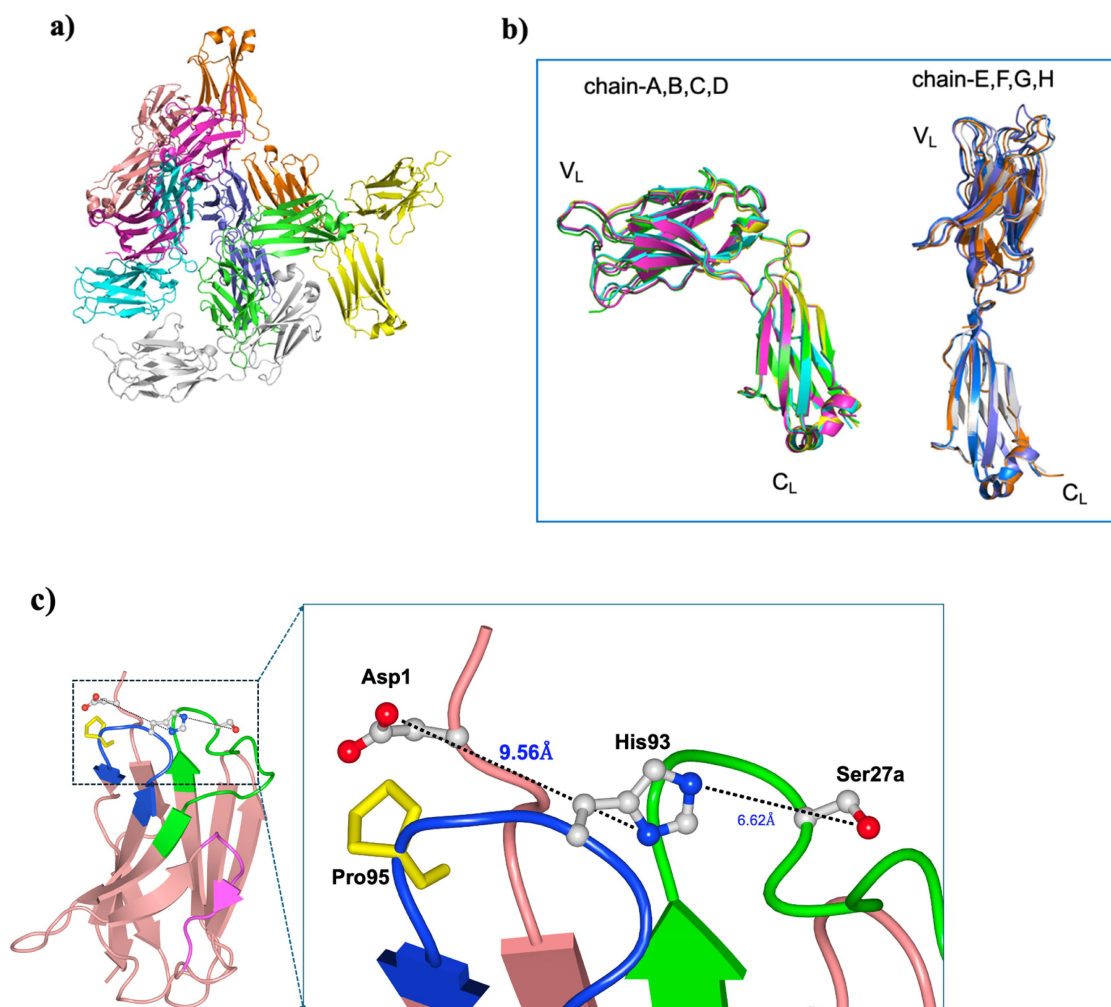| clone	K_D (M)	ka = ($M^{-1}s^{-1}$)(x10)	k_d = (s^{-1})(x10^{-3})
T99wt	4.43×10^{-8}	3.73 ± 0.07	1.67 ± 0.06
T99-Pro95(-)	3.35×10^{-8}	4.03 ± 0.08	1.35 ± 0.06

Figure 4. 3D-structure of T99wt. The crystal structure of T99wt was resolved at a 2.6 Å resolution. (a) Eight molecules in the asymmetric unit. Structure of each full-length T99wt molecule is presented with a different color. (b) Among the eight molecules, we observed two types of molecules with different conformations: bending (molecules A, B, C, and D) and straight (molecules E, F, G, and H). VL; variable region of light chain CL; constant region of light chain (c) The structure of the variable region is shown on the left. Enlarged view is presented on the right: CDR-1(green), CDR-3 (blue). The distance between Asp1 (Oδ1)-His93 (Nδ1) is 9.56 Å and that between His93 (Nε2) and Ser27a (Oγ) is 6.62 Å.

Table 2. Distances of Cα among Asp1-His93-Ser27a (Å).

T99		Asp1	His93	Ser27a
T99wt	Mol A	7.5		9.8
	Mol B	7.6		9.4
	Mol C	8.3		10.2
	Mol D	7.6		9.4
	Mol E	8.5		10.4
	Mol F	8.1		9.9
	Mol G	7.9		9.5
	Mol H	7.8		10.2
	Average	**7.9**		**9.9**

(Mol A is closest to the Average); (Kabat's numbering).

presence or absence of Pro95. This positioning of His93 is assumed to be critical for catalytic function, contributing to the formation of a catalytic site in the T99-Pro95(-) variant.

Molecular dynamic simulation

The structures obtained from X-ray crystallography represented the lowest-energy conformational states of the molecules. However, molecular flexibility and conformational dynamics play crucial roles in solution-phase behavior. To capture these dynamic features, we conducted MD simulations of the antibody light chains, focusing on the Asp1-Ser27a-His93 region. Based on X-ray crystallography-derived structural data under conditions mimicking the molecular environment, these simulations provide insights into the conformational mobility and local interactions within this key region.

MD simulations of T99wt and T99-Pro95(-) were conducted under three different conditions, each based on the protonation states of His27d and His93.

Structural analysis of the catalytic domain

The MD simulations were performed to observe the structural motion of the full-length T99wt and T99-Pro95(-) light chains, with a particular focus on the catalytic domain. The X-ray crystallography results confirmed the importance of His93. In these simulations, we also examined the behavior of His27d, which occasionally contributes to the formation of a catalytic triad,[8,20] alongside His93, to explore the underlying factors that confer the dominance of His93 in catalytic
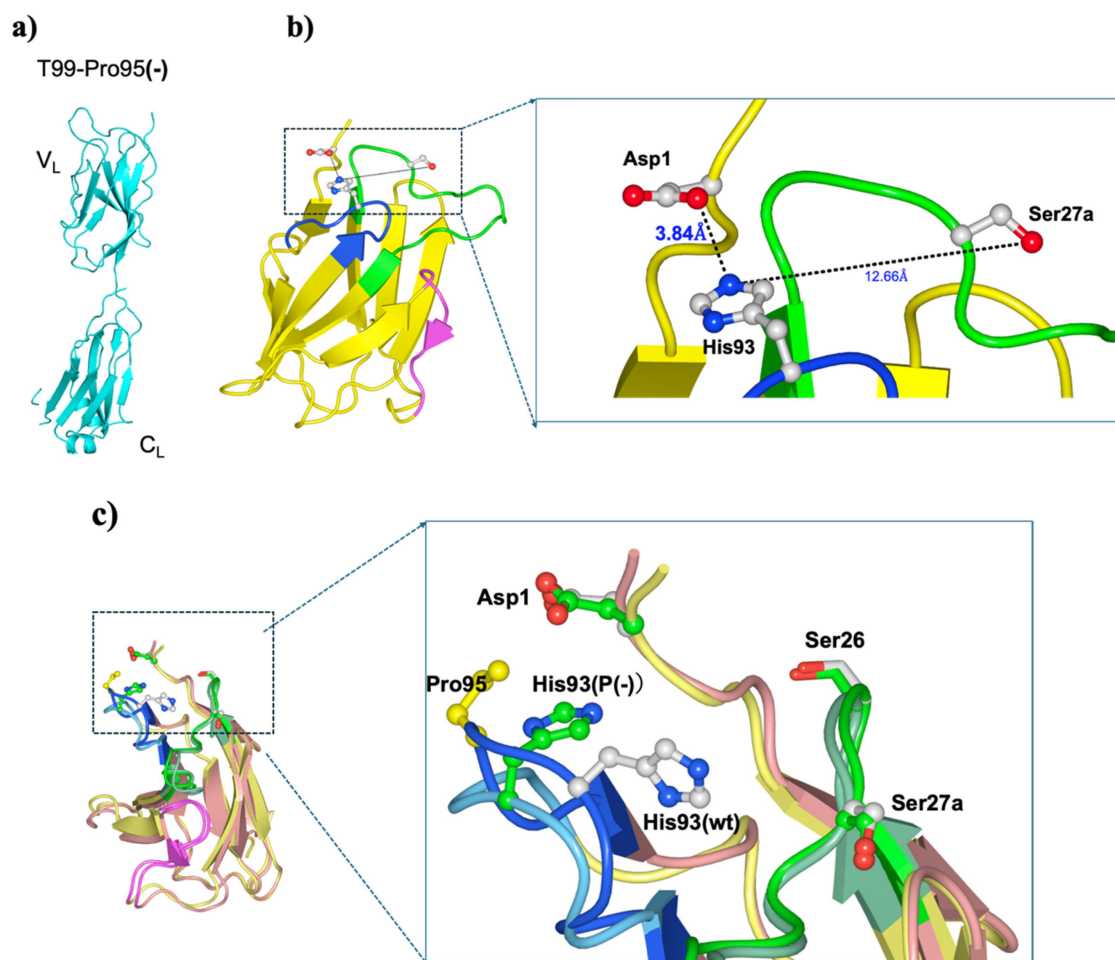
Figure 5. 3D-structure of T99-Pro95(-). The structure of T99-Pro95(-) has been resolved at a 2.0 Å resolution. (a) One molecule in the asymmetric unit. The structure of the full-length T99-Pro95(-) is presented. This is a straightforward type. (b) Structure of the variable region. An enlarged view is presented on the right-hand side (CDR-1; green, CDR-3; blue). The distances between Asp1 (Oδ1)-His93 (Nε2) is 3.84 Å and that between His93 (Nε2) and Ser27a (Oγ) is 12.66 Å. Note that the distance between Asp1-His93 of T99-Pro95(-) became shorter by 5.71 Å compared to that of T99wt. (c) Superimposed view: T99wt, backbone (light red); CDR-1 (green), CDR-3 (blue) Amino acid residues: T99wt; gray, T99-Pro95(-); green, Proline; yellow

function. In addition, examining the different protonation states of His27 and His93 helps capture potential variations in protein behavior and stability. Histidine residues are particularly influential in protein structure and function, as their pK_a values are close to the physiological pH, enabling them to act as proton donors or acceptors. By analyzing three configurations, the non-protonated state with neutral His (i; H27d/H93) and single protonated state at either His27 or His93 (ii; H27dH$^+$/H93 and iii; H27d/H93H$^+$), we can evaluate how these protonation states impact structural dynamics, molecular interactions, or the solvent-accessible surface area (SASA) around the catalytic region. These effects may influence the functional behavior of proteins under different conditions.

SASA and root mean square deviation (RMSD) analyses (Figures 6a and S2) indicated that T99wt exhibits greater fluctuations than T99-Pro95 (-) across the MD trajectory, particularly in the (i) His27d/His93 system. T99wt exhibited higher SASA fluctuations, with increased flexibility and solvent exposure, likely due to the effects of the His27d and His93 protonation states and the presence of Pro95 (Figure 6a), whereas T99-Pro95 (-) appeared to be more stable. The average structures revealed that the catalytic domain had a limited area of stability in T99wt compared to that in T99-Pro95(-) (Figures 6b,c). The Asp1-His27d distance was also larger in T99wt (19.36 Å) than in T99-Pro95(-) (15.33 Å), with Asp1, His27d, and His93 exhibiting substantial fluctuations. Reduced solvent exposure may create a more hydrophobic and rigid active site, enhancing substrate binding, limiting water interference, and stabilizing the transition state for more efficient catalysis.

Notably, in T99wt, Asp1 frequently moved outward from the central catalytic region and rarely entered it. However, in T99-Pro95(-), His93 initially remained outside this region but shifted toward Ser27a after 10 ns, followed by the Asp1 approach near 17.5–18.5 ns, suggesting a potential close interaction configuration (See Fig. S2-S3 and Movie S1a – S1d in Supporting Information). Additionally, principal component analysis (PCA) of the last 50 ns further highlighted the distinct motion patterns between T99wt and T99-Pro95 (-) (Figure 6d).
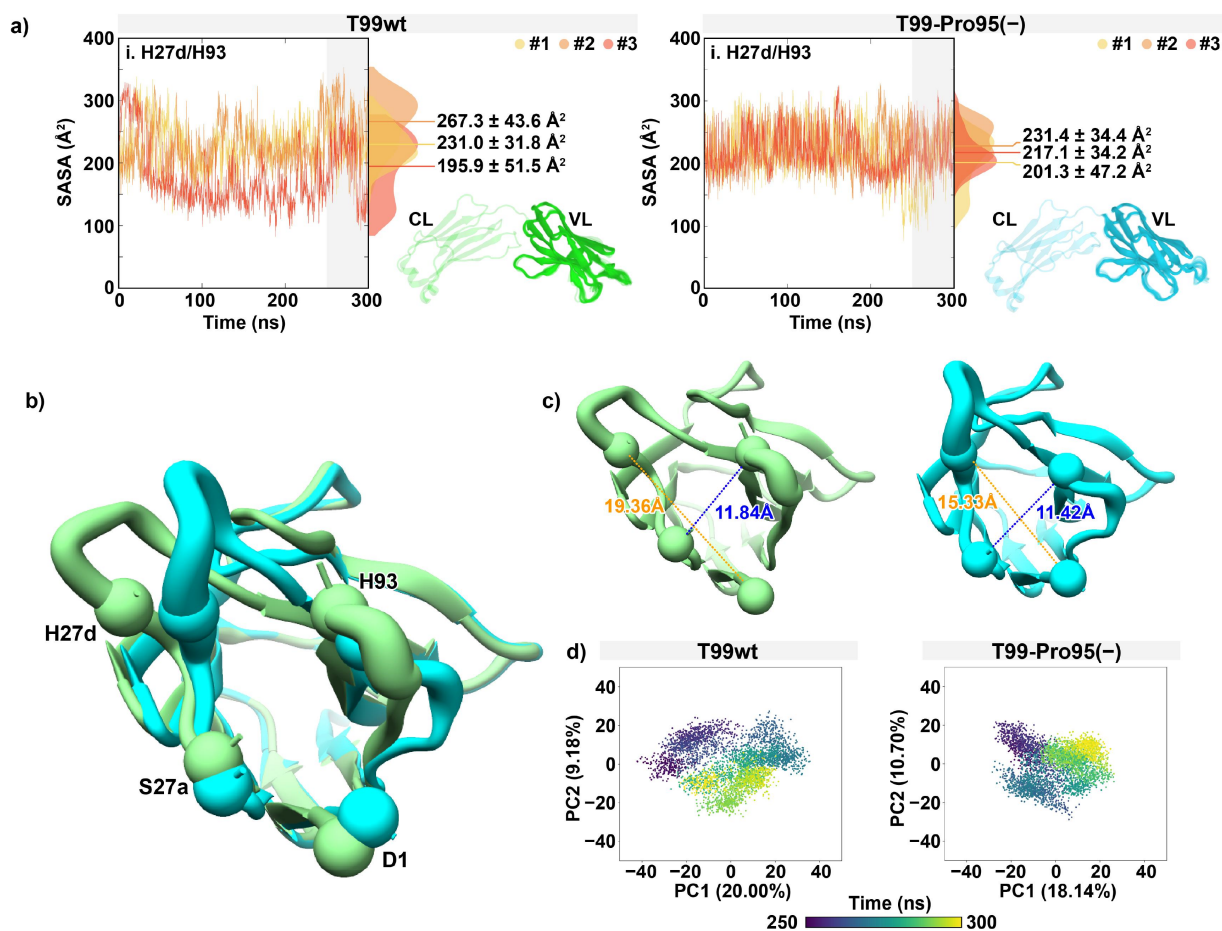
Figure 6. Structural and dynamic analysis of the T99wt and T99-Pro95(-) catalytic domains. (a) Solvent-accessible surface area (SASA) of T99wt and T99-Pro95(-) at residues His27d and His93, highlighting the catalytic domain with key residues Asp1, Ser27a, and His93. The density plot displays data from the last 50 ns of MD trajectories across three independent runs. The 3D structures of T99wt (green) and T99-Pro95(-) (cyan) show the entire protein, including the constant (CL) and variable (VL) regions. (b) Superimposed structures of the T99wt and T99-Pro95(-) catalytic domains. (c) The representative structures extracted from the last snapshot of the MD simulation are plotted for the distances between residues Asp1-His27d and Ser27a-His93, which are depicted with blue and orange dashed lines, respectively. (d) Principal component analysis (PCA) of the last 50 ns of the MD trajectories for each system. Residues Asp1, Ser27a, His27d, and His93 are marked as spheres in all structural representations.

Structural stability and flexibility

The two-dimensional free energy landscape (2D FEL) revealed significant differences in the conformational stability and flexibility between the two systems (Figure 7a). In the T99-Pro95(-) system, the global minimum state exhibited a more restricted and narrow chemical search space for (i) His27d/His93 than for the other protonation states (ii) His27dH⁺/His93, and (iii) His27d/His93H⁺. This result suggests the highly stable conformation of T99-Pro95(-) under these conditions. The distance between Oδ1 of Asp1 and Nε2 of His93 (dD1$^{O\delta1}$ ... H93$^{N\varepsilon2}$) remained at a 5 Å diameter throughout the MD simulation in T99-Pro95(-), indicating minimal fluctuation. In contrast, the T99wt system exhibited a broader distribution, fluctuating between 5 Å and 11 Å, forming two distinct clusters across three independent runs. These results suggest a higher degree of flexibility in T99wt compared to T99-Pro95(-). This result indicated that they hardly formed the catalytic triad of Asp1, Ser27a, and His93, which is consistent with the X-ray crystallography results.

In the (ii) and (iii) His27d/His93H⁺ systems, both T99wt and T99-Pro95(-) displayed the broadest free energy landscape, indicating more conformational freedom and higher fluctuation. In T99wt, the overall protein fluctuation is substantial, but due to the hydrophobic interaction with Pro95, His93 cannot approach Asp1. In contrast, in T99Pro95(-), the absence of Pro95 prevents the formation of a hydrophobic interaction with His93. This increases the fluctuation of His93, allowing it to approach Asp1. Protonation at His93 appears to play a significant role in increasing the flexibility of the system, as seen in the broader 2D FEL for the (iii) His27d/His93H⁺ state. These results are consistent with the RMSD profiles of these systems (Fig. S3).

Discussion

As previously reported,[26,28] an amino acid residue Pro95 is a highly conserved residue even though it resides in the CDR-3 of the antibody light chain. Surprisingly, an existing antibody can be converted into the corresponding catalytic antibody by deleting the Pro95 residue (and/or the proline residue(s) close to Pro95).[24] This approach represents a significant advancement over conventional methods for generating catalytic antibodies
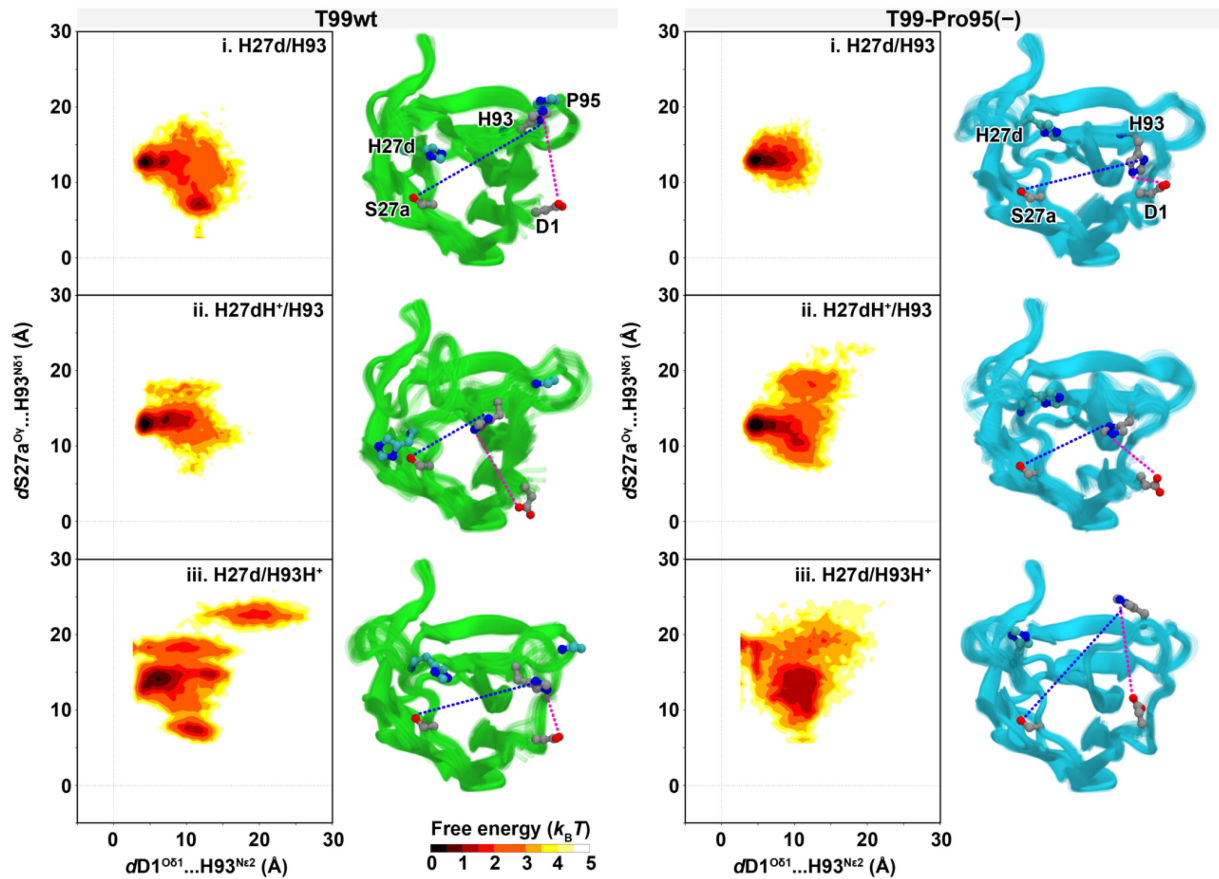
Figure 7. Molecular dynamics/ two-dimensional free energy calculation. Two-dimensional free energy landscape (2D FEL) of T99wt and T99-Pro95(-) for (i) His27d/isH93, (ii) His27dH$^+$/His93, and (iii) His27d/His93H$^+$, plotted based on the distance between Oδ1 of D1 and Nε2 of H93 (dD1^{Oδ1}...H93^{Nε2}) on the x-axis, and Oγ of Ser27a and Nδ1 of H93 (dS27a^{Oγ}...H93^{Nδ1}) on the y-axis. The free-energy scale ranged from 0 to 5 k_BT. The superimposition structure extracted from the last 50 ns-MD trajectories is illustrated along with the 2D-FEL.

because we can produce catalytic antibodies more efficiently and rapidly compared to conventional ones. However, the underlying mechanism by which the Pro95-deleted antibody is able to acquire the catalytic function has not been elucidated until now. Therefore, in this study, we investigated the biochemical and structural differences between antibodies with and without Pro95.

The T99 light chain belongs to the germline gene Vk2–29 × 02 in subgroup II of the human kappa light chain, which encodes a catalytic triad-like structure composed of Asp1-Ser27a-His93 (or His27d).[1,10,11,16,20,23] The proportion of Vk2–29 germline is about 0.4% of 3,794 cDNA kappa sequences annotated in IMGT. Its residues can function as catalytic sites if placed in an appropriate position and under appropriate conditions.

Considering the above explanation, donanemab and/or lecanemab, whose light chain belongs to the above germline gene, may be considered potential catalytic antibody candidates for amyloid-β clearance.

In the case of T99wt, the Aβ peptide cannot be cleaved owing to the lack of catalytic activity. However, the Pro95 deleted variant (T99-Pro95(-)) was able to cleave both the FRET-Aβ peptide and Aβ (1–40) molecule.[24] The only difference between these two molecules was the presence or absence of Pro95. Based on the X-ray crystallography analysis, we discovered that the deletion of Pro95 reduces the distance between the functional group of Asp1-His93 from

9.56 Å (T99wt) to 3.84 Å (T99-Pro95 (-)), as shown in Figure 5c. Although residues such as Asp1 and Ser27a did not change their location and configuration, His93 of T99-Pro95(-) was shifted several angstroms toward Asp1. No other changes were observed in the crystal structure. This significant change is related to the formation of a catalytic site in T99-Pro95(-).

According to molecular modeling, the distance between Asp1(Oδ1) and His93(Nδ1) was 8.67 Å in T99wt and 5.71 Å in T99-Pro95(−). In X-ray crystallographic analysis, the distance between Asp1(Oδ1) and His93(Nδ1) was 9.56 Å in T99wt, while that between Asp1(Oδ1) and His93(Nε2) was 3.84 Å in T99-Pro95(-). Both analyses showed a consistent trend.

As the distance between His93 and Ser27a is 12.66 Å (Figure 5b,c), it is possible that Ser26 plays a role in a catalytic site instead of Ser27, because the distance to His93 is shortened to 7.39 Å.

Regarding the binding kinetics study, the K_D values of T99wt and T99-Pro95(-) were 4.43 and $3.35 × 10^{-8}$ (M), respectively. The values of ka are 3.73 and 4.03 (M^{-1}s^{-1})(x 10^4). This difference is less than 10%. On the other hand, kd values are 1.67 and 1.35 (s^{-1} ×10^{-3}) for each respective clone, representing a difference of approximately 20%. It is assumed that antigen dissociation is more difficult in the Pro-deleted variant, suggesting that the catalytic site may retain the antigen

for a longer period compared to the wild type. Considering that the similar K_D values between T99wt and T99-Pro95(-), the deletion of Pro95 in CDR-3 does not directly correlate with the antigen recognition ability.

MD simulation also provided additional insights into the higher activity of T99-Pro95 (-) compared to that of T99wt. An important finding was the larger molecular motion of the Asp1 and His93 residues, while that of Ser27a was small (Figure 6a-d). Significant fluctuations in Asp1 were expected owing to its location at the N-terminus. The presence of Pro95 in T99wt introduced hydrophobic contact interactions with His93, which restricted the molecular motion of His93 and potentially reduced its catalytic efficiency. However, the large movement of His93 in T99-Pro95(-) resulted in the generation of a catalytic site, which is an interesting phenomenon.

The 2D FEL revealed that T99-Pro95(-) adopted a more stable and restricted conformation, minimizing fluctuations in the catalytic region and preserving a consistent distance between important residues, such as Asp1 and His93. In contrast, T99wt exhibited broader fluctuations, which may destabilize the catalytic sites and impair catalytic efficiency.

SASA analysis further supported these observations, as T99-Pro95 (-) exhibited a more insulated and less solvent-exposed catalytic pocket, shielding the active site from disruptive solvent interactions (Figure 6). These combined factors suggest that T99-Pro95(-) forms a more rigid and efficient catalytic environment, leading to higher enzymatic activity than T99wt. The flexibility of His93 observed in T99-Pro95 (-) suggests that its protonation state could influence catalytic activity. Given His93's role in proton transfer, pH-dependent catalysis is likely relevant under physiological conditions and may modulate enzyme efficiency. The pKa values of His27d and His93, calculated from MD-averaged structures, shifted closer to physiological pH in T99-Pro95(–) compared to T99wt, supporting a more favorable protonation state for catalysis. Additionally, Trp94, positioned next to His93, shows greater conformational flexibility in T99-Pro95(-) due to the absence of Pro95, which in T99wt forms stabilizing hydrophobic contacts. This increased mobility allows His93 to sample conformations closer to Asp1 and Ser27a, contributing to a more catalytically favorable active site.

The formation of a catalytic site by deleting Pro95 is necessarily for the conversion stated above. There are many kinds of catalytic sites, for example Asp-Ser-His (Trypsin), Gln-Ser-Lys (β-Lactamase), and Glu-Ser-His (Acetyl Cholinesterase), in natural enzymes. In addition, in the case of antibodies, the presence of some kinds of catalytic sites, such as triads[2,17,18,23,31] and dyads,[27,35,36] among others,[28,37] have been reported. The amino acids forming a catalytic site preferably come close to each other, which can be achieved by the structural change like deletion of Pro95. Considering that the conversion of mouse antibody light chains into catalytic antibody light chains was successfully achieved,[38] the Pro95-deletion strategy is likely to be applicable in many cases. Incidentally, approximately **5%** of the therapeutic antibodies use the Vk2–29 germline (the clones are humanized) and all the antibodies possess Pro95 residue. It will be important to determine how the Pro-deletion strategy can be applied to other germline genes.

In conclusion, this study resolves the long-standing question of why Pro95-deleted antibodies acquire catalytic activity. Structural analysis using X-ray crystallography and MD simulations demonstrated that His residues play a crucial role in catalytic site formation, which strongly correlates with the biochemical properties of both catalytic and non-catalytic antibodies.

Materials and methods

Reagents

Chemical reagents such as Tris, glycine, $CuCl_2 \cdot 2 h_2O$, $ZnSO_4 \cdot 7 h_2O$, KCl, $Na_2HPO_4 \cdot 12 h_2O$, NaCl, KH_2PO_4, EDTA·2Na and IPTG were purchased from Wako Pure Chemical Industries Ltd., Osaka, Japan (Guaranteed Reagent). Synthetic peptides of Arg-pNA (Precisely, Bz-L-Arg-pNA·HCl), Glu-pNA, Ala-pNA, Phe-Leu-pNA and Gly-Pro-pNA) were purchased from Peptide Institute Inc., Osaka, Japan. Tryptone and yeast extract were purchased from Becton-Dickinson and Company, NJ, USA.

Synthesis of fluorescence resonance energy transfer (FRET) substrates

The FRET-Aβ substrate (7-MCA-SNKGAIIGK(DNP)rrr-NH_2) was synthesized as follows; the Aβ26–33 sequence with 7-MCA, K(DNP), and (D-Arg)$_3$ was constructed on a Rink amide resin by the standard 9-fluorenylmethoxy-carbonyl protocol.[24] For the FRET-Tau peptide, the sequence of 391–408 of the Tau protein was selected. The peptide was chemically modified by attaching MCA to the N-terminus and DNP to the C-terminus. The resulting modified sequence is 7-MCA-EIVYK(pS)PVVSGDT(pS) PRHLK(DNP)-NH₂, where pS indicates phosphorylated serine residues. The peptide resin was treated with trifluoroacetic acid-H_2O-phenol-thioanisole-ethanedithiol (82.5:5:5:5:2.5) at room temperature for 2 hr. After removal of the resin by filtration, cold diethyl ether was added to the solution to afford a precipitate, which was collected by centrifugation and washed with diethyl ether. The crude peptide was purified by reversed-phase HPLC (RP-HPLC) on a Waters DELTA 600 system, incorporating the 2487 UV/visible detector (Waters, Milford, MA). The HPLC-purified peptide (retention time: 30.23 min; Cosmosil type: 5C18-AR-2 (4.6 × 250 mm); milliQ water in 0.05% trifluoroacetic acid (TFA): acetonitrile in 0.05% TFA from 90:10 to 30:70 in 60 min (1.0 mL/min)) was characterized by electrospray ionization mass spectrometry.

Amplification of DNA fragments encoding light chains from germline genes of subgroup II

T99wt light chains

Preparation of the human kappa light chain genes (T99wt) were performed in accordance with that described in references 17, 19, and 20. Briefly stated, peripheral blood lymphocytes obtained from healthy volunteers were harvested using a Ficoll-Paque (GE Healthcare UK Ltd.,

Buckinghamshire, England) gradient, and stored appropriately. Total RNA was prepared from 3.0×10^7 cells using an RNA isolation kit (Stratagene, La Jolla, CA, USA) for synthesizing cDNA. Oligo (dT) was used for reverse transcription PCR using the total RNA as a template (ThermoScript RT-PCR System; Invitrogen, Carlsbad, CA, USA). To prepare T-series human antibody light chain belonging to kappa subgroup II used in this study, we used a two-step PCR technique. At the first step, a DNA fragment was amplified using the primers as a forward primer 5'-CCTGGGGCTGCTAATC-3', and a reverse primer 5'-ACACTCTCCCCTGTTGAAG-3'. The PCR reaction occurred under the following incubation conditions: 30 seconds at 98°C, 29 cycles of 10 seconds at 98°C for denaturation, 30 seconds at 63.5 C (or 67°C) for annealing, and 30 seconds at 72°C for extension. Finally, the extension was carried out for 5 minutes at 72°C. At the second step, the following primers were used as a forward primer 5'-acgctaccatgGATATTGTGATGACTCAGTCT-3' and a reverse primer 5'-atggtactcgagACACTCTCCCCTGTTG -3'. The PCR reaction occurred under the following incubation conditions: 30 seconds at 98°C, 25 cycles of 10 seconds at 98°C for denaturation, 30 seconds at 62.8°C for annealing, and 30 seconds at 72°C for extension. Finally, the extension was carried out for 5 minutes at 72°C. In the PCR, a restricted enzyme, Phusion (High-Fidelity DNA Polymerase, Finnzyme, Finland), was used.

The amplified DNA fragment was separated by 3% agarose gel electrophoresis. The fragment of the expected size was extracted using a QIAquick Gel Extraction Kit (Qiagen, Valencia, CA, USA). Purified PCR product was directly ligated to pET20b (+) vector (Novagen, Madison, WI, USA), which was repurified and transformed into BL21 (DE3)pLysS for expression of light chains.

Construct of T99-Pro95(-)

Deletion of Pro95 from the wild type of T99 (T99wt) was performed by the method of inverse PCR using as the reverse primer 5'-CCAGTGTGTACCTTGCATGCAGT-3' and the forward primer 5'-GGGACTTTCGGCCCTGGGA-3'. In the experiment, KOD-Plus-Mutagenesis Kit (TOYOBO, Code SMK-101, Osaka) was used and the construct was firstly transformed to DH5α and finally to BL21(DE3)pLysS for the expression.

Culture, recovery and purification

The transformant was grown at 37 °C in 1 liter of Luria-Bertani medium containing 100 μg/ml ampicillin to an A600 nm of 0.6 and then incubated with 0.01 mm IPTG for 20 h at 18 °C. Cells were harvested by centrifugation (3500 g, 4°C, 10 min) and then resuspended in a 100 mL solution of 250 mm NaCl, 25 mm Tris-HCl, pH 8.0). The cells were lysed by ultrasonication three times for 2 min each in an ice bath, followed by centrifugation (17,800 g, 4°C, 20 min). The expressed human light chain was recovered as the supernatant.

The supernatant was first subjected to Ni-NTA column chromatography (Takara, Otsu, Japan) equilibrated with 25 mm Tris-HCl, pH 8.0, containing 250 mm NaCl. Elution was performed by increasing the concentration of imidazole from 0 and/or 30 to 300 mm.

After the Ni-NTA column chromatography was completed, an aliquot of a solution of 50 μM $CuCl_2$ (1.25–2.0 eq. for the light chain) was added into the eluent, based on the calculation that the absorbance of A280 nm of 1.0 in UV/VIS was regarded as ~1 mg/mL (40 μM light chain). Then, the solution including the light chain and copper ion was dialyzed against a 50 mm Tris-HCl buffer, pH 8.0, for about 20 hr. After removing some aggregates by centrifugation (17,800 g, 4°C, 20 min), the solution was concentrated to 2 mg/mL and subjected to a cation-exchange chromatography using a column of SP-5PW (TOSOH, Japan) with a gradient of NaCl (from 0.0% to 15.0%) in Tris-HCl (pH 8.0) buffer on the purification apparatus (AKTA system, GE-Healthcare-Japan, Tokyo). Then, the eluent (as a flow-through) was recovered and submitted to dialysis against 20 mm Tris-HCl/150 mm NaCl buffer (pH 8.5) for about 17 hr, then concentrated using Amicon ultra10000 (Millipore, USA). EDTA was added the solution to a concentration of 50 mm and allowed to react for 1 hr at 4°C, followed by dialysis against 2 L of PBS (pH 7.4), twice (1st was for 5 hr and 2nd for 16 hr). After confirming the complete removal of Cu(II) by UV/VIS spectroscopy, it was filtered using a 0.2 μm membrane filter (Merck-Millipore) and stored at 4°C or frozen.

Protein concentrations were determined by the Bradford method using a Lowry method using the DC protein assay kit (Bio-Rad).

Sequencing

T99wt and T99-Pro95(-) clones were sequenced with an ABI 3730×l Analyzer (Applied Biosystems, CA, USA) by using ABI BigDye™ Terminator v3.1 Cycle Sequencing Kits. GENETIX Ver. 8 (GENETIX, Tokyo, Japan) software was used for sequence analysis and deduction of amino acid sequences.

Cleavage assays

To avoid contamination in cleavage assays, the glassware, plastic ware, and buffer solutions used in this experiment were sterilized as much as possible by heating (180°C, 2 hr), autoclaving (121°C, 20 min), or filtration through a 0.20-μm sterilized filter. The experiments were mostly performed in a biological safety cabinet to avoid airborne contamination.

Cleavage of the amide bond linking pNA to C-terminal amino acid in peptidyl-pNA substrates such as Arg-pNA, Glu-pNA, Ala-pNA, Phe-Leu-pNA, and Gly-Pro-pNA (Peptides Institute Inc., Osaka, Japan) was measured at 37°C in Glycine/Tris buffer containing 0.025% Tween20 (TGT buffer containing 0.02% sodium azide; pH 7.7) in 96-well plates (96-well plate/353075, Becton-Dickinson, NJ, USA). Purified light chain (10 μL) was mixed with 90 μL of each synthetic substrate solution. The final concentration of the light chain and the substrate was 5 μM and 50 μM, respectively. pNA released from the substrate catalyzed by the light chain was detected by measurement of the absorbance at 405 nm, while 620 nm was used as the reference using a micro-plate reader (Scanlt 3.1 for Multiskan FC, ThermoFisher Scientific, MA, USA). The

peptidase activity of catalytic antibodies was estimated by the concentration of released pNA.

The FRET-Aβ or FRET-Tau substrates (25 µM) was incubated with the purified T99wt or T99-Pro95(-) (5 µM) in 50 mm/Tris-100 mm/Glycine-Tween25 (TGT buffer containing 0.02% sodium azide, pH7.7, at 37°C. Fluorescence was measured periodically on the Fluoroskan Ascent ($\lambda_{ex} = 320$ nm and $\lambda_{em} = 405$ nm; Thermo Fisher Scientific Oy, Vantaa, Finland) for up to 72 hr. All measurements were done in duplicate.

Binding affinity

The binding affinity of T99wt and T99-Pro95(-) to amyloid-beta was measured by using an Octet N1 (Sartorius AG, Germany) and Advanced Kinetics method in accordance with the protocol. Streptavidin fixed biosensor-tip (SA-biosensor) was used to fix the amyloid-beta molecule with biotin-tag (ASI Anaspec; AS-23523-05). The experiment followed a five-step sequential assay at room temperature. First, a SA-biosensor was dipped in a PBS buffer (250 µL) in a microtube (ClickFit, LightBlock, PP, Black, 0.5 mL, TreffLab, Degersheim, Switzerland) for 30 s, and then the SA-biosensor was dipped in a Drop-Holder containing 4 µL of 250 nM of amyloid-beta with biotin-tag for 120 s. At the third step, the SA-biosensor (immobilized with an amyloid-beta molecule with biotin-tag) was dipped in the PBS of the microtube for washing. At the fourth step, the Amyloid-beta immobilized SA-biosensor was applied in a drop-holder containing 4 µL of an antibody solution to associate with the antibody for 120 s, and, at final (fifth) step, the SA-biosensor bound with antibody was again dipped in a PBS buffer to measure the dissociation. The results (K_D, ka and kd) were calculated by Octet N1 software (version 1.4.0.13) using a global fitting. In this experiment, various concentrations of each antibody were prepared to obtain accurate evaluation of the binding affinity (K_D,) the association value (ka) and the dissociation value (kd). The binding affinity (K_D) was calculated by kd/ka.

X-ray crystallography

The initial crystallization screening was carried out by using an automated crystallization system.[39] After crystallization condition refinement, the crystals of T99wt were grown in 10 mg/ml T99wt protein, 14% (w/v) PG3350, 0.4 M KSCN, 0.1 M HEPES (pH7.5) and 30% (v/v) glycerol at 20°C by vapor diffusion method. X-ray diffraction data were collected at BL-5A (Photon Factory, KEK) at 1.0000 Å. The data were processed using the HKL2000 system.[40] The initial phase was determined by the molecular replacement method with the program Molrep[41] using the structure of L-chain of Fab for integrin binding protein (PDB code: 4HCR) as a search model. The model automatically constructed using Crank2[42] was refined using Phenix.[43] The data collection and refinement statistics are listed in supporting Table S1.

T99-Pro95(-) protein (5 mg/ml) was mixed with 0.5% CoCage-1[44] and 1 mm SNKGAIIGK peptide which worked as crystallization additives and subjected to crystallization. The crystals were grown in 0.1 M sodium cacodylate (pH 6.5) and 36% PEG2000MME at 4°C by vapor diffusion method. X-ray diffraction data were collected at BL32XU (SPring-8) at 1.0000 Å. Multiple data were collected by ZOO system[45] and merged by KAMO.[46] The data were integrated by XDS[47] and scaled by Xscale. The phase was determined by the molecular replacement method by Phaser[48] using the structure of T99wt as a search model.

Molecular modeling

The deduced antibody light-chain amino acid sequences were used for computational analysis of the antibody structures using Discovery Studio (Accelrys, Inc., San Diego, CA, USA). For homology modeling, template structures were created using a BLAST search, following minimization of the total energy of the molecule using the CHARMM algorithm. The resulting Protein Data Bank data were used to modify the complementarity-determining region (CDR) structures defined using the Kabat numbering system.

Molecular dynamics simulation

The 3D structures of T99wt and T99-Pro95(-) from X-ray crystallography were used for MD simulations. Protonation states at pH 7.0 were assigned using PDB2PQR,[49] creating three systems for each protein based on the protonation states of His27 and His93, including (i) H27d/H93, (ii) H27dH$^+$/H93, and (iii) H27d/H93H$^+$. Hydrogen atoms and ions were added, and the structures were solvated in a TIP3P water[50] box with a 15 Å from the protein's surface in a cubic box. These steps were performed using the tLEaP module in AmberTools24,[51] as previously described.[52–54] Energy minimization was then carried out with 5,000 steps of the steepest descent/conjugate gradient algorithm, followed by heating to 300 K under the NVT ensemble for 1 ns. Each system was simulated for 300 ns at 300 K with three independent replicates using PMEMD.cuda in AMBER24,[55] under the NPT ensemble, totaling 12 systems. MD trajectories were analyzed for structural stability, including RMSD, SASA, and PCA, as well as free energy landscapes using CPPTRAJ[56] in AmberTools24 and PyEMMA.[57] Structural superimpositions extracted from the last 50 ns of (i) H27d/H93 and plots were visualized with VMD 1.9.4,[58] and Matplotlib,[59] in an in-house Python script.

Statistical analysis

Correlation and standard deviation analyses were performed using Microsoft Excel for Mac (version 16.66.1).

Acknowledgments

Disclosure statement

Funding

ORCID

Taizo Uda http://orcid.org/0000-0001-8146-7902
Hiroaki Taguchi http://orcid.org/0000-0003-3183-6380
Emi Hifumi http://orcid.org/0000-0002-5123-3846

Abbreviations

aa	amino acid
Aβ	amyloid-beta
CBB	Coomassie brilliant blue
CDRL-3	CDR-3 of light chain
2D FEL	two-dimensional free energy landscape
DNP	2,4-dinitrophenyl
eq	equivalent
FRET	Förster resonance energy transfer
HPLC	high-performance liquid chromatography
IPTG	isopropyl-β-D-thiogalactopyranoside
mAb	monoclonal antibody
7-MCA	(7-methoxycoumarin-4-yl)acetyl
MD	molecular dynamics
MS	mass spectroscopy
ns	nano second
PCA	principal component analysis
PBS	phosphate-buffered saline
RMSD	root mean square deviation
R-pNA	Benzoyl-L-arginine p-nitroanilide monohydrochloride
SASA	solvent-accessible surface area
TGT	50mM /Tris-100mM /Glycine-Tween-20 buffer
TFA	trifluoroacetic acid
UV/VIS	ultraviolet-visible spectroscopy

Author contributions

TU, RK, YS, and EH designed the study; TU, RK, YS, JK, HY, MaT, KH, MoT and HT performed the experiments; TU, RK, YS, HK, MoT, and EH analyzed the data; TU, RK, YS, SH, HT and EH supervised the study and wrote the manuscript.

Data and materials availability

The data supporting this study are available from the corresponding author upon request. The atomic coordinates of T99wt and T99-Pro95 (-) were deposited in the Protein Data Bank under the accession codes 8ZNT and 8ZNU, respectively. The plasmids are available from the corresponding author upon request. The source data are provided in this study.

References

1. Gao QS, Sun M, Tyutyulkova S, Webster D, Rees A, Tramontano A, Massey RJ, Paul S. Molecular cloning of a proteolytic antibody light chain. J Biol Chem. 1994;269 (51):32389–32393. doi: 10.1016/S0021-9258(18)31647-8.
2. Mei S, Mody B, Eklund SH, Paul S. Vasoactive intestinal peptide hydrolysis by antibody light chains. J Biol Chem. 1991;266 (24):15571–15574. doi: 10.1016/S0021-9258(18)98440-1.
3. Parkhomenko TA, Buneva VN, Tyshkevich OB, Generalov II, Doronin BM, Nevinsky GA. DNA-hydrolyzing activity of IgG antibodies from the sera of patients with tick-borne encephalitis. Biochimie. 2010;92(5):545–554. doi: 10.1016/j.biochi.2010.01.022.
4. Krasnorutskii MA, Buneva VN, Nevinsky GA. DNase, RNase, and phosphatase activities of antibodies formed upon immunization by DNA, DNase I, and DNase II. Biochem (Mosc). 2011;76 (9):1065–1072. doi: 10.1134/S0006297911090124.
5. Xia Y, Eryilmaz E, Zhang Q, Cowburn D, Putterman C. Anti-DNA antibody mediated catalysis is isotype dependent. Mol Immunol. 2016;69:33–43. doi: 10.1016/j.molimm.2015.11.001.
6. Lacroix-Desmazes S, Moreau A, Sooryanarayana Bonnemain C, Pashov N, Stieltjes A, Hoebeke Y, Sultan J, Kazatchkine MD, Kaveri SV, Kaveri SV. Catalytic activity of antibodies against factor VIII in patients with hemophilia a. Nat Med. 1999;5(9):1044–1047. doi: 10.1038/12483.
7. Ponomarenko NA, Durova OM, Vorobiev II, Belogurov AA, Kurkova IN, Petrenko AG, Telegin GB, Suchkov SV, Kiselev SL, Lagarkova MA, et al. Autoantibodies to myelin basic protein catalyze site-specific degradation of their antigen. Proc Natl Acad Sci USA. 2006;103(2):281–286. doi: 10.1073/pnas.0509849103.
8. Mitsuda Y, Hifumi E, Tsuruhata K, Fujinami H, Yamamoto N, Uda T. Catalytic antibody light chain capable of cleaving a chemokine receptor CCR-5 peptide with a high reaction rate constant. Biotechnol Bioeng. 2004;86(2):217–225. doi: 10.1002/bit.20031.
9. Hifumi E, Higashi K, Uda T. Catalytic digestion of human tumor necrosis factor-α by antibody heavy chain. FEBS J. 2010;277 (18):3823–3832. doi: 10.1111/j.1742-4658.2010.07785.x.
10. Sharma V, Heriot W, Trisler K, Smider V. A human germ line antibody light chain with hydrolytic properties associated with multimerization status. J Biol Chem. 2009;284(48):33079–33087. doi: 10.1074/jbc.M109.036087.
11. Hifumi E, Mitsuda Y, Ohara K, Uda T. Targeted destruction of the HIV-1 coat protein gp41 by a catalytic antibody light chain. J Immunological Methods. 2002;269(1–2):283–298. doi: 10.1016/S0022-1759(02)00242-9.
12. Hifumi E, Hatiuchi K, Okuda T, Nishizono A, Okamura Y, Uda T. Specific degradation of H. pylori urease by a catalytic antibody light chain. FEBS J. 2005;272(17):4497–4505. doi: 10.1111/j.1742-4658.2005.04869.x.
13. Taguchi H, Planque S, Nishiyama Y, Symersky J, Boivin S, Szabo P, Friedland RP, Ramsland PA, Edmundson AB, Weksler ME, et al. Autoantibody-catalyzed hydrolysis of amyloid β peptide. Journal Of Biological Chemistry. 2008;283(8):4714–4722. doi: 10.1074/jbc.M707983200.
14. Planque SA, Nishiyama Y, Sonoda S, Lin Y, Taguchi H, Hara M, Kolodziej S, Mitsuda Y, Gonzalez V, Sait HB, et al. Specific amyloid β clearance by a catalytic antibody construct. J Biol Chem. 2015;290(16):10229–10241. doi: 10.1074/jbc.M115.641738.
15. Paul S, Karle S, Planque S, Taguchi H, Salas M, Nishiyama Y, Handy B, Hunter R, Edmundson A, Hanson C. Naturally occurring proteolytic antibodies: selective immunoglobulin M-catalyzed hydrolysis of HIV gp120. J Biol Chem. 2004;279(38):39611–39619. doi: 10.1074/jbc.M406719200.
16. Uda T, Hifumi E. Super catalytic antibody and antigenase. J Biosci Bioeng. 2004;97(3):143–152. doi: 10.1016/S1389-1723(04)70183-8.
17. Hifumi E, Honjo E, Fujimoto N, Arakawa M, Nishizono A, Uda T. Highly efficient method of preparing human catalytic antibody light chains and their biological characteristics. FASEB J. 2012;26 (4):1607–1615. doi: 10.1096/fj.11-195339.
18. Hifumi E, Takao S, Fujimoto N, Uda T. Catalytic and biochemical features of a monoclonal antibody heavy chain, JN1-2, raised against a synthetic peptide with a hemagglutinin molecule of

influenza virus. J Am Chem Soc. 2011;133(38):15015–15024. doi: 10.1021/ja203922r.

19. Hifumi E, Fujimoto N, Arakawa M, Saito E, Matsumoto S, Kobayashi N, Uda T. Biochemical features of a catalytic antibody light chain, 22F6, prepared from human lymphocytes. J Biol Chem. 2013;288(27):19558–19568. doi: 10.1074/jbc.M113.454579.

20. Hifumi E, Arakawa M, Matsumoto S, Yamamoto T, Katayama Y, Uda T. Biochemical features and antiviral activity of a monomeric catalytic antibody light-chain 23D4 against influenza a virus. FASEB J. 2015;29(6):2347–2358. doi: 10.1096/fj.14-264275.

21. Bowen A, Wear MP, Cordero RJ, Oscarson S, Casadevall A. A monoclonal antibody to Cryptococcus neoformans glucuronoxylomannan manifests hydrolytic activity for both peptides and polysaccharides. J Biol Chem. 2017;292(2):417–434. doi: 10.1074/jbc.M116.767582.

22. Hifumi E, Arakawa M, Uda T. Frontiers in clinical drug research-anti infectives. In: Atta-Ur R. editor. Preparation and perspectives of catalytic antibodies possessing characteristic ability to inhibit infection against viruses such as influenza and rabies. Vol. 4. Bentham Science Publishers; 2017. p. 28–57. doi: 10.2174/9781681084879117040004.

23. Hifumi E, Morihara F, Hatiuchi K, Okuda T, Nishizono A, Uda T. Catalytic features and eradication ability of antibody light-chain UA15-L against Helicobacter pylori. J Biol Chem. 2008;283 (2):899–907. doi: 10.1074/jbc.M705674200.

24. Hifumi E, Taguchi H, Tsuda H, Minagawa T, Nonaka T, Uda T. A new algorithm to convert a normal antibody into the corresponding catalytic antibody. Sci Adv. 2020;6(13):eaay6441. doi: 10.1126/sciadv.aay6441.

25. Köhler G, Milstein C. Continuous cultures of fused cells secreting antibody of predefined specificity. Nature. 1975;256 (5517):495–497. doi: 10.1038/256495a0.

26. Hifumi E, Taguchi H, Nonaka T, Uda T. Direct conversion of a general antibody to its catalytic antibody and corresponding applications —importance and role of Pro95 in CDR-3—. Proc J Acad Ser B. 2023;99(6):155–172. doi: 10.2183/pjab.99.010.

27. Kolesnikov AV, Kozyr AV, Alexandrova ES, Koralewski F, Demin AV, Titov MI, Avalle B, Tramontano A, Paul S, Thomas D, et al. Enzyme mimicry by the antiidiotypic antibody approach. Proc Natl Acad Sci USA. 2000;97(25):13526–13531. doi: 10.1073/pnas.200360497.

28. Hifumi E, Nonaka T, Taguchi H, Uda T. A new catalytic site functioning in antigen cleavage by H34 catalytic antibody light chain. Sci Rep. 2022;12(1):19185. doi: 10.1038/s41598-022-23689-6.

29. Matsuura K, Yamamoto K, Sinohara H. Amidase activity of human Bence Jones proteins. Biochem Biophys Res Commun. 1994;204(1):57–62. doi: 10.1006/bbrc.1994.2425.

30. Matsuura K, Ohara K, Munakata H, Hifumi E, Uda T. Pathogenicity of catalytic antibodies: catalytic activity of Bence Jones proteins from myeloma patients with renal impairment can elicit cytotoxic effects. Biol Chem. 2006;387(5):543–548. doi: 10.1515/BC.2006.070.

31. Okochi N, Kato-Murai M, Kadonosono T, Ueda M. Design of a serine protease-like catalytic triad on an antibody light chain displayed on the yeast cell surface. Appl Microbiol Biotechnol. 2007;77(3):597–603. doi: 10.1007/s00253-007-1197-0.

32. Durova OM, Vorobiev II, Smirnov IV, Reshetnyak AV, Telegin GB, Shamborant OG, Orlova NA, Genkin DD, Bacon A, Ponomarenko NA, et al. Strategies for induction of catalytic antibodies toward HIV-1 glycoprotein gp120 in autoimmune prone mice. Mol Immunol. 2009;47(1):87–95. doi: 10.1016/j.molimm.2008.12.020.

33. Thiagarajan P, Dannenbring R, Matsuura K, Tramontano A, Gololobov G, Paul S. Monoclonal antibody light chain with pro-thrombinase activity. Biochemistry. 2000;39(21):6459–6465. doi: 10.1021/bi992588w.

34. Dai CL, Tung YC, Liu F, Gong CX, a Iqbal K. Tau passive immunization inhibits not only tau but also Aβ pathology. Alzheimers Res Ther. 2017;9(1):1. doi: 10.1186/s13195-016-0227-5.

35. Paetzel M, Dalbey RE. Catalytic hydroxyl/amine dyads within serine proteases. Trends Biochem Sci. 1997;22(1):28–31. doi: 10.1016/S0968-0004(96)10065-7.

36. Liao DI, Breddam K, Sweet RM, Bullock T, Remington SJ. Refined atomic model of wheat serine carboxypeptidase II at 2.2-A resolution. Biochemistry. 1992;31(40):9796–9812. doi: 10.1021/bi00155a037.

37. Kim YR, Kim JS, Lee SH, Lee WR, Sohn JN, Chung YC, Shim HK, Lee SC, Kwon MH, Kim YS. Heavy and light chain variable single domains of an anti-DNA binding antibody hydrolyze both double- and single-stranded DNAs without sequence specificity. J Biol Chem. 2006;281 (22):15287–15295. doi: 10.1074/jbc.M600937200.

38. Hifumi E, Ito Y, Tsujita M, Taguchi H, Uda T. Enzymatization of mouse monoclonal antibodies to the corresponding catalytic antibodies. Sci Rep. 2024;14(1):12184. doi: 10.1038/s41598-024-63116-6.

39. Kato R, Hiraki M, Yamada Y, Tanabe M, Senda T. A fully automated crystallization apparatus for small protein quantities. Acta Crystallogr F Struct Biol Commun. 2021;77(1):29–36. doi: 10.1107/S2053230X20015514.

40. Otwinowski Z, Minor W. Processing of X-ray diffraction data collected in oscillation mode. Methods Enzymol. 1997;276:307–326.

41. Vagin A, Teplyakov A. MOLREP: an automated program for molecular replacement. J Appl Crystallogr. 1997;30 (6):1022–1025. doi: 10.1107/S0021889897006766.

42. Skubák P, Pannu NS. Automatic protein structure solution from weak X-ray data. Nat Commun. 2013;4(1):2777. doi: 10.1038/ncomms3777.

43. Liebschner D, Afonine PV, Baker ML, Bunkóczi G, Chen VB, Croll TI, Hintze B, Hung LW, Jain S, McCoy AJ, et al. Macromolecular structure determination using X-rays, neutrons and electrons: recent developments in Phenix. Acta Crystallogr D Struct Biol. 2019;75(10):861–877. doi: 10.1107/S2059798319011471.

44. Yao M, Li L. Nucleant enhancing nucleation of a protein crystal and protein crystallization method with the same. Justia Pat. 2020;20210130400.

45. Hirata K, Yamashita K, Ueno G, Kawano Y, Hasegawa K, Kumasaka T, Yamamoto M. ZOO: an automatic data-collection system for high-throughput structure analysis in protein microcrystallography. Acta Crystallogr D Struct Biol. 2019;75 (2):138–150. doi: 10.1107/S2059798318017795.

46. Yamashita K, Hirata K, Yamamoto M. KAMO: towards automated data processing for microcrystals. Acta Crystallogr D Struct Biol. 2018;74(5):441–449. doi: 10.1107/S2059798318004576.

47. Kabsch W. XDS. Acta Crystallogr D Biol Crystallogr. 2010;66 (2):125–132. doi: 10.1107/S0907444909047337.

48. McCoy AJ, Grosse-Kunstleve RW, Adams PD, Winn MD, Storoni LC, Read RJ. Phaser crystallographic software. J Appl Crystallogr. 2007;40(4):658–674. doi: 10.1107/S0021889807021206.

49. Dolinsky TJ, Nielsen JE, McCammon JA, Baker NA. PDB2PQR: an automated pipeline for the setup of poisson-Boltzmann electrostatics calculations. Nucleic Acids Research. 2004;32(Web Server): W665–667. doi: 10.1093/nar/gkh381.

50. Mark P, Nilsson L. Structure and dynamics of the TIP3P, SPC, and SPC/E water models at 298 K. J Phys Chem A. 2001;105 (43):9954–9960. doi: 10.1021/jp003020w.

51. Case DA, Aktulga HM, Belfon K, Cerutti DS, Cisneros GA, Cruzeiro VW, Forouzesh N, Giese TJ, Götz AW, Gohlke H, et al. AmberTools. J Chem Inf Model. 2023;63(20):6183–6191. doi: 10.1021/acs.jcim.3c01153.

52. Hengphasatporn K, Wilasluck P, Deetanya P, Wangkanont K, Chavasiri W, Visitchanakun P, Leelahavanichkul A, Paunrat W, Boonyasuppayakorn S, Rungrotmongkol T, et al. Halogenated Baicalein as a promising antiviral agent toward SARS-CoV-2 main protease. J Chem Inf Model. 2022;62(6):1498–1509. doi: 10.1021/acs.jcim.1c01304.

53. Hengphasatporn K, Aiebchun T, Mahalapbutr P, Auepattanapong A, Khaikate O, Choowongkomon K, Kuhakarn C, Meesin J, Shigeta Y, Rungrotmongkol T. Sulfonylated Indeno[1,2-c]quinoline derivatives as potent EGFR tyrosine kinase inhibitors. ACS Omega. 2023;8(22):19645–19655. doi: 10.1021/acsomega.3c01195.

54. Duan L, Hengphasatporn K, Sakai T, Fujiki R, Yoshida N, Hirota S, Shigeta Y. Why is dimeric 3D Domain swapping in antibody light chains missing from the solution? Atomistic insights mechanisms. J Phys Chem B. 2024;128(38):9086–9093. doi: 10.1021/acs.jpcb.4c03234.

55. Case DA, Aktulga HM, Belfon K, Ben-Shalom IY, Berryman JT, Brozell SR, Cerutti DS, Cheatham TI, Cisneros GA, Cruzeiro VWD, et al. Amber. San Francisco: University of California; 2024.

56. Roe DR, Cheatham TE. PTRAJ and CPPTRAJ: software for processing and analysis of molecular dynamics trajectory data. J Chem Theory Comput. 2013;9(7):3084–3095. doi: 10.1021/ct400341p.

57. Senne M, Trendelkamp-Schroer B, Mey AS, Schütte C, Noé F. EMMA: a software package for Markov Model building and analysis. J Chem Theory Comput. 2012;8(7):2223–2238. doi: 10.1021/ct300274u.

58. Humphrey W, Dalke A, Schulten K. VMD: visual molecular dynamics. J Mol Graph. 1996;14(1):33–38, 27–38. doi: 10.1016/0263-7855(96)00018-5.

59. Hunter JD. Matplotlib: a 2D graphics environment. Comput Sci Eng. 2007;9(3):90–95. doi: 10.1109/MCSE.2007.55.